Published online August 22, 2006

Reproduced from Soil Science Society of America Journal. Published by Soil Science Society of America. All copyrights reserved.

Nanoscale Biogeocomplexity of the Organomineral Assemblage in Soil: Application of STXM Microscopy and C 1s-NEXAFS Spectroscopy

James Kinyangi, Dawit Solomon, Biqing Liang, Mirna Lerotic, Sue Wirick, and Johannes Lehmann*

ABSTRACT

Methodological constraints limit the extent to which existing soil aggregation models explain carbon (C) stabilization in soil. We hypothesize that the physical infrastructure of microaggregates plays a major role in determining the chemistry of the occluded C and intimate associations between particulate C, chemically stabilized C and the soil mineral matrix. We employed synchrotron-based scanning transmission X-ray microscopy (STXM) coupled with near-edge X-ray absorption fine structure (C 1s-NEXAFS) spectroscopy to investigate the nanoscale physical assemblage and C chemistry of 150-μm microaggregates from a Kenyan Oxisol. Ultra-thin sections were obtained after embedding microaggregates in a sulfur block and sectioning on a cryo-microtome at −55°C. Principal component and cluster analyses revealed four spatially distinct features: pore surfaces, mineral matter, organic matter, and their mixtures. The occurrence of these features did not vary between exterior and interior locations; however, the degree of oxidation decreased while the complexity and occurrence of aliphatic C forms increased from exterior to interior regions of the microaggregate. At both locations, compositional mapping rendered a nanoscale distribution of oxidized C clogging pores and coating pore cavities on mineral surface. Hydrophobic organic matter of aromatic and aliphatic nature, representing particulate C forms appeared physically occluded in 2- to 5-μm pore spaces. Our findings demonstrate that organic matter in microaggregates may be found as either oxidized C associated with mineral surfaces or aromatic and aliphatic C in particulate form. Using STXM and C 1s-NEXAFS we are for the first time able to resolve the nanoscale biogeocomplexity of unaltered soil microaggregates.

Long-term stabilization of soil organic matter (SOM) is controlled by structural configurations in the organomineral assemblage of soil microaggregates (Tisdall, 1996; Bronick and Lal, 2005). Several processes combining knowledge of soil parent material, microaggregate structures, and biogenic feedback mechanisms are suggested to explain the form and function of soil aggregates as well as the existence of an aggregate hierarchy in soil (Tisdall and Oades, 1982; Oades and Waters, 1991). Many studies apply model experiments to evaluate the effects of cultivation on soil aggregation (Six et al., 2004) and C stabilization in various fractions of SOM (Guggenberger et al., 1994; Kaiser et al., 2002). In a review, Blanco-Canqui and Lal (2004), discuss how the development of such models will facilitate better understanding of C sequestration in soils. Since most conceptual models are built on evidence collected from destructive SOM tests, they fail to explicitly provide a linkage to spatial functionality of C stabilization occurring in microaggregate pore regions. This shortcoming is attributed in part to the slow advancement of methodological approaches addressing the functional relevance of SOM (Elliott et al., 1996; Sohi et al., 2001; Wander, 2004). Although progress in scanning electron microscopy (Mikutta et al., 2004), computer microtomography (Albee et al., 2000) and X-ray scattering techniques (Amelung et al., 2002; Leifeld and Kögel-Knabner, 2003) now render images of internal microaggregate porosities and their intra-aggregate attributes, the spatial interrelationships between soil C forms and aggregate stability are still largely unknown.

Application of microspectroscopy to study the structure of biomaterials (Warwick et al., 1998; Hitchcock et al., 2002), now affords the opportunity to adapt novel techniques to investigate nanoscale processes in the C chemistry and structural assembly of soil aggregates. Recent attempts by Schmidt et al. (2003) show that microspectroscopy can be used to capture the microscale variability of SOM in hydrated soil samples dispersed in aqueous media. In an attempt to elucidate the surface C functional characteristics of 5- to 80-μm size black carbon (BC) particles, Lehmann et al. (2005) succeeded to prepare 200-nm thin BC sections for X-ray microscopy and spectroscopic imaging. In this approach, a combination of STXM is accomplished in conjunction with NEXAFS to study the nanoscale distribution of C forms on particle surfaces in soil. Incident photon energy is increased throughout a C absorption K edge (280 eV), beyond the ionization threshold (290 eV) causing excited core electrons to be removed from the core hole and promoted to a continuum. The excited phase of the inner-core electron (1s) is characteristic of the structure of the C molecular bonding and can be correlated to specific C forms (Ade et al., 1992; Stöhr, 1992). Multiple C 1s electron transitions in the NEXAFS region (284 eV-290 eV) reveal the presence of C moieties such as aromatic-C (C=C), aliphatic-C (C–H), carboxyl-C (COOH), and carbonyl-C (C=O).

Synchrotron STXM and C 1s-NEXAFS are widely used to resolve nanostructures of polymers (Smith et al., 2001) and to fingerprint C in biological materials (Lerotic et al., 2004; Hitchcock et al., 2005), where radiation exposure is controlled to avoid damage to the susceptible C = O bond (Braun et al., 2005). High concentrations of C (>700 g C kg^{-1}) in uniform polymer layered samples (Ade and Urquhart, 2002) and BC (Lehmann et al., 2005)

J. Kinyangi, D. Solomon, B. Liang, and J. Lehmann, Dep. of Crop and Soil Sci., Cornell Univ., Ithaca, NY 14853; M. Lerotic and S. Wirick, Dep. of Physics and Astronomy, State University of New York, Stony Brook, NY 11794. Received 17 Oct. 2005. *Corresponding author (CL273@cornell.edu).

Published in Soil Sci. Soc. Am. J. 70:1708–1718 (2006).
Soil Chemistry
doi:10.2136/sssaj2005.0351
© Soil Science Society of America
677 S. Segoe Rd., Madison, WI 53711 USA

Abbreviations: BC, black carbon; CM-I*o*, mineral background; OD, optical density; PS-I*o*, pore space background; SOM, soil organic matter; SVD, singular value decomposition.

Reproduced from Soil Science Society of America Journal. Published by Soil Science Society of America. All copyrights reserved.

permit NEXAFS data filtering, thereby improving the signal/noise ratio of the images. Solomon et al. (2005) also showed that processing extracts through a 2-μm pore membrane to trap mineral particles enhances C spectral signal response from humic substances containing 300 to 500 g C kg^{-1}. Currently, it is difficult to examine organic matter in soils that contain minerals and low amounts of C (5–150 g C kg^{-1}) because its micro-scale spatial distribution is highly heterogeneous. In this case, the C 1s signal response is significantly masked by absorbance interferences from mineral matter. We attempted to use STXM and C 1s-NEXAFS to investigate C chemical forms in mineral-pore structures after modifying the data background correction. In applying STXM and C 1s-NEXAFS, our objectives were: (i) to examine structural features that confer stabilization of C in the microaggregate soil assemblage; and (ii) to determine the spatial distribution of C chemical functional forms on surfaces and interior regions of unaltered soil microaggregates.

MATERIALS AND METHODS

Site and Soil Sample Background

We obtained soil aggregate material from an agricultural field located on a heavy textured Oxisol (Soil Survey Staff, 2003) dominated by 1:1 kaolinite clays adjacent to Kakamega forest (34° 57′ 14″E Lat.; 00° 14′ 20″N Long.; 1733 m above sea level) in western Kenya. The site is part of a chronosequence experiment, investigating the long-term effects of cultivation agriculture on soil organic matter degradation. The area receives 2080 mm of annual rainfall in a bimodal distribution with a mean annual temperature of 19.0°C. A 1-kg soil sample from a cultivated maize field that had recently (2001) been converted from natural primary forest was collected from 0.1-m depth using a core sampler with a diameter of 0.1 m. Before sampling in June 2003, the site had been tilled for five seasons and planted to maize (*Zea mays* L.) and bean (*Phaseolus vulgaris* L.) crops. The soil was air-dried, crushed, and passed through a 2-mm sieve, packed and submitted to the laboratory. Soil properties for the soil sample were: 85.6 g C kg^{-1}, 9.8 g N kg^{-1}, and 1.9 g S kg^{-1}, and pH $_{KCL}$ of 5.3. Other soil chemical and mineralogical properties for Kakamega forest are reported in a study by Krull et al. (2002). They characterize these soils to be dominated by silica, Fe, and Al, with low base status (Ca, K, and Mg) due to intense weathering and confirmed the absence of calcite by XRD analysis.

Preparation of Microaggregate Thin Sections

In our previous work (Lehmann et al., 2005), we reported a procedure for identifying and ultra-sectioning (Ultracut UTC, Leica Microsystems Inc. Bannockburn, IL, USA) 5- to 80-μm BC particles embedded in preheated (220°C) and super-cooled (in liquid N_2) elemental sulfur before sample image and spectroscopic analysis. Several attempts to apply this protocol to section soil aggregates < 250 μm were unsuccessful, partly due to the collapse of the crumb structure of soil aggregates under the pressure of the microtome knife. We modified the sectioning protocol to include soil aggregate pretreatment. Specifically, a 1-g soil sample was sieved to pass a 250-μm screen to obtain microaggregates, then sprinkled on a glass fiber filter (Whatman GF/A, 47 mm, 1.6 μm opening), mounted onto a sieve surface and fixed to a chimney funnel that transferred warm mist from a humidifier (Ultra-violet light, Slant/Fin; 7.5L capacity). The humidifier chamber was filled with water dispensed from a Barnstead NanoPure Diamond water purification system. After 18 h of continuous misting, the microaggregates were considered to be water saturated. Excess droplets on the glass fiber filter were drained off before freezing microaggregates. A 150-μm microaggregate subsample was selected, embedded in a sulfur block and submitted to the cryo-microtome for sectioning. Since the pretreatment resulted in a frozen sample, sectioning was accomplished at −55°C. For a detailed description of the cryo-microtome features and thin section sample operations, see Lehmann et al. (2005).

After sectioning, several microaggregate thin slices were mounted on Cu grids (200 mesh, no 53002, Ladd Research, Williston, VT, USA) impregnated with silicon monoxide (SiO) substrate. The grid was mounted onto the center pinhole of stainless steel sample stage plates (46-mm diam.) with tape to hold the edge. The microaggregate was secured in the crystalline structure of sulfur that was then sublimed in a vacuum oven (1 h, 40°C, 3.1 MPa), before measurement. Because specificity of the C chemistry relies on the contrast in absorption between successive features of the sample images, the section thickness must be controlled to minimize error. To optimize the signal/noise ratio, Ade et al. (1992) recommend that C-based material (1 g cm^{-3}) be sectioned between 40 and 800 nm thick, whereas Boese (1996) estimate 1 μm to be the typical thickness of biological samples prepared for spectromicroscopy. In this study, microaggregates were sectioned to ~800-nm thickness. The C content was low (<100 g C kg^{-1} soil) because aggregates also consist of dense mineral matter (>2 g cm^{-3}). For comparison, protein density is about 1.35 g cm^{-3} (Boese, 1996).

STXM and C 1s NEXAFS Data Acquisition

Scanning transmission X-ray microscopy and C 1s-NEXAFS spectroscopic measurements were completed at beamline X1A1 of the National Synchrotron Light Source, Brookhaven National Laboratory. This light source produces a soft X-ray beam from the 2.8 GeV electron storage ring, which illuminates a monochromator that is tunable over 250 to 800 eV, operated in synchrony with the sample z-stage. The z-stage was adjusted to focus the X-rays through the microaggregate sample section. Slit openings were set at 25/30/25 μm giving an energy resolution of 0.1 eV. When combined, the slit settings and zone plate provided scanning spatial resolution of 50 nm. The monochromator energy was increased from 280 to 282.5 eV in 0.3 eV increments (scan time 1 msec), from 282.5 to 292 eV in 0.1 eV steps (scan time 3 msec), and from 292 to 310 eV in 0.3 eV steps (scan time 3 msec). Smaller energy steps of 0.1 eV were chosen in the spectroscopic regions where C 1s core electron excitation is indicative of sharp 1s $\rightarrow\pi^*$, and broad 1s, 3p $\rightarrow\sigma^*$ transitions. The scan time was increased to reduce error and improve recorded data. Single images were recorded from succeeding photon energy levels and built into a stack using the program Stack Analyze 2.6.1 (Jacobsen et al., 2000). Alignment was completed from a constant reference energy level at 280 eV using the cross-correlation matrix, constrained to a shift limit of 30 pixels, after sobel routine adjustment for edge enhancement. Further stack image processing software and data analyses instructional manuals can be accessed on the website at http://xray1.physics.sunysb.edu/data/software.php.

Principle Component Analyses

We used the program PCA_GUI 1.1.1 (http://xray1.physics.sunysb.edu/data/software.php) to orthogonalize and noise-filter data. X-ray image data were separated into three significant

Reproduced from Soil Science Society of America Journal. Published by Soil Science Society of America. All copyrights reserved.

components (s = 1, 2, 3) describing the main features in the microaggregate sample because prior knowledge of such features was unknown. Significant components were determined based on observations of the eigenvalues, eigenimage, and eigenspectra (Beauchemin et al., 2002; Lerotic et al., 2004). The goal was to select components due to systematic variations of spectral signals from pixel to pixel and to discard random fluctuations of signal beyond which noise effects will occur. The eigenspectra of the component would be flat, implying lack of variation due to chemical speciation (Lerotic et al., 2004). The eigenimage scaling factor was adjusted between 0.3 and 0.6 to increase sensitivity only when additional cluster searches did not control high OD signal responses from pixel classification of minerals.

Cluster Pixel Classification

In PCA_GUI 1.1.1, we performed cluster analyses to classify regions in the sample according to spectral similarities of pixel groupings. Using the intensity values from the background (Io) histogram, a region of high flux indicated by the brightest surface in the image was selected (PS-Io). Several iterated runs improved the accuracy of Io region selection through observing the optical density of the designated Io surface, adjusted to near 0. Since our sample contained minerals, organic matter, and their mixtures, we found strong interference on the filtering of spectral signals that could in part be attributed to ultra-thin regions of optically less dense mineral flakes that are detached from the assemblage. Such regions were classified more due to their OD than spectral characteristics. This resulted in a large pre-edge absorbance as previously noted by Smith et al. (2001), during their examination of polymer material with high chloride contents. Because mineral and pore space pixels occupy the vast majority of the spectral signal search space, pixels due to organic matter were grouped most distant away from their cluster centers. This grouping indicated poor classification by the euclidean algorithm, thereby rendering average cluster spectra that were poorly resolved in definition, whose energy peak positions were difficult to assign.

Composition Thickness Maps

Subsequent to principal component and cluster analyses, singular value decomposition (SVD) was calculated, providing compositional thickness maps from corresponding fitted data. Because SVD is computed from matrix inversion procedures (Koprinarov et al., 2002; Lerotic et al., 2004), it is possible to derive equivalent thickness maps leading to variation in sample mineral and C pseudo-thickness. Optical density is a distinct feature of NEXAFS, which is calculated from the transmitted X-ray intensities where sample scan images (I) are normalized from an Io scan event recorded without the sample (Jacobsen et al., 2000). The Beer-Lambert law is used to quantify absorption (A) where:

$$A = \mathrm{OD} = \mu(E)\rho T = -\ln(I/I_{\mathrm{O}}), \quad [1]$$

with

$$T = \mathrm{OD} / \mu(E)\rho, \quad [2]$$

given that μ is a mass absorption coefficient at energy level E, ρ is the material density, and T is the sample thickness.

This composition permits construction of thickness maps (Koprinarov et al., 2002; Lerotic et al., 2004), which represent cluster spectra of C forms and those that define regions of mineral and pore spaces. Maps that were uncorrelated with spatial features and only exhibited random patterns were removed from the analysis. Map elimination was based on dissimilarity in classified pixels obtained from cluster analyses. The most contrasting cluster pixel groupings were identified and only these were sought in the composition thickness maps. While this approach allowed us to decompose the major themes expressed in the microaggregate assemblage, we caution that multiple functional forms in the C chemistry often remain embedded in single thematic regions, causing a compositional overlay in the map thickness. Because boundary regions are indiscrete (Lerotic et al., 2004), we argue that spectral composition areas must always be viewed as spatial gradations where C forms transition in functional characteristics. During map elimination, care must be taken to retain such overlay regions because they certainly correspond to unique C chemical features.

To further interpret structural features in the STXM image and associated NEXAFS data, a direct linear relationship was assumed between absorbance in photon energy (OD) and sample material density (Eq. [1]). When sample section thickness T for a given density ρ varied in optical depth with respect to the incident soft X-ray beam, we expected OD in the energy absorbance to change. We interpreted this change of variation in the signal response to denote unique sample density characteristics (Koprinarov et al., 2002). We used knowledge of the conceptual features in the microaggregate assemblage (Fig. 1), absorbance characteristics (Eq. [1], Eq. [2]), and the cluster display of all spectra (not shown) to approximate the OD ranges that correspond to organic matter, minerals, and their mixtures (Table 1).

RESULTS AND DISCUSSION

STXM Microscopy

Microaggregate regions showed much variation in their material density of C and mineral matter. However, the presence of visible internal mesopore networks permitted transmission of the soft X-ray beam and C density maps (Fig. 2c and 3c) were inferred from the resulting–log ratio of the images (Fig. 2a, 2b, 3a, and 3b). Optical densities in the resolved spectral regions for mineral and

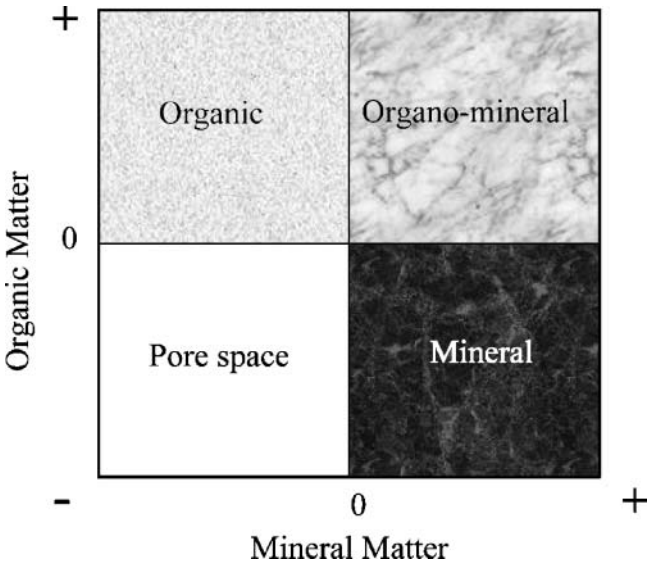

Fig. 1. Conceptual framework for the interplay between minerals, organic matter, and pore space determining the C stabilization in the soil organomineral assemblage.

Reproduced from Soil Science Society of America Journal. Published by Soil Science Society of America. All copyrights reserved.

Table 1. Relationships between aggregate features, optical densities (OD) and the C compositional expression from spectral signal dominance of the interior and exterior regions of a soil microaggregate.

		C 1s binding energy transition					
Feature	OD	$\pi^*_{C=C}$	$\pi^*_{C=N}$	π^*_{C-H}	π^*_{COOH}	$\sigma^*_{C=O}$	Dominant C bond
Pore space	< 0.5	−†	−	−	−	−	none (OD near 0)
Organic	0.5–1.0	+++‡	++	++	+++	++	C=C, C–H, C=O
Organomineral	1.0-1.8	++	−	−	+++	++	COOH, C=N, C=O
Mineral	> 1.8	−	−	−	−	−	none (OD near 2.5)

† No detectable C functional form (−).
‡ Carbon functional form less dominant (+), dominant (++) and most dominant (+++) in the absorption spectrum.

organomineral matter were elevated, not so much due to sample physical thickness (T), but rather in response to variation in the material density (ρ). Such density heterogeneity is not uncommon in complex biological material (Smith et al., 2001; Hitchcock et al., 2005). By combining STXM and NEXAFS measurements, we were able to extract micro variation to map C molecular composition with high spatial resolutions of up to 50 nm. In addition, C, mineral and pore assemblage features were resolved without altering the physical structure of the microaggregate.

NEXAFS I*o* Background Correction

We classified spectral regions by varying the ratio of significant components to cluster search by a factor of 3 to 4 (2/3–2/12 for PS-I*o* and 2/6–2/18 for CM-I*o*), where I*o* background regions correspond to pore space (PS) or mineral matter (CM). This search was combined with cluster composition mapping to investigate variations in the C chemistry and mineral composition. When PS-I*o* was selected for correction, the pixel population was tightly anchored around clusters of mineral absorbance that contain OD values > 2.0 (Table 1). Pixels that represent mixtures of mineral and organic matter were distinctly clustered further away from clay and separated from pixel clusters of organic matter. Although pixel clusters of pore space needed to correspond to OD values near 0, we noticed elevated values particularly when few cluster regions were sought (Fig. 4b). Lerotic et al. (2004) have suggested the use of angle rather than euclidian distance measure algorithm to improve clustering where physical thickness variations interfere with composition resolution. Because we find both physical thickness and density variations to be inherent properties of organomineral interactions, an algorithm that suppresses density variations would almost lead to loss in optical compositional prediction. Instead, we used the euclidian distance measure approach to classify the microaggregate sample pixel population to capture both density and C chemical variations that result from organomineral associations.

Given that a slight energy shift in peak position can mean a complete alteration in the C chemistry (Scheinost et al., 2001), we sought alternative analyses to correct for poor peak definition arising from large background interference by mineral matter. We used a pixel classification that instead designates mineral absorbance regions of high OD as the I*o*, without masking expression of mineral or organomineral pixels. This approach is a modification to cluster data filtering for those biological and environmental samples that not only contain low C contents, but also include areas where C is occluded in dense non-C matter. This modification corrects for elevated preedge absorbance and minor variations unrelated to OD, which improves cluster centering of carbonaceous pixels

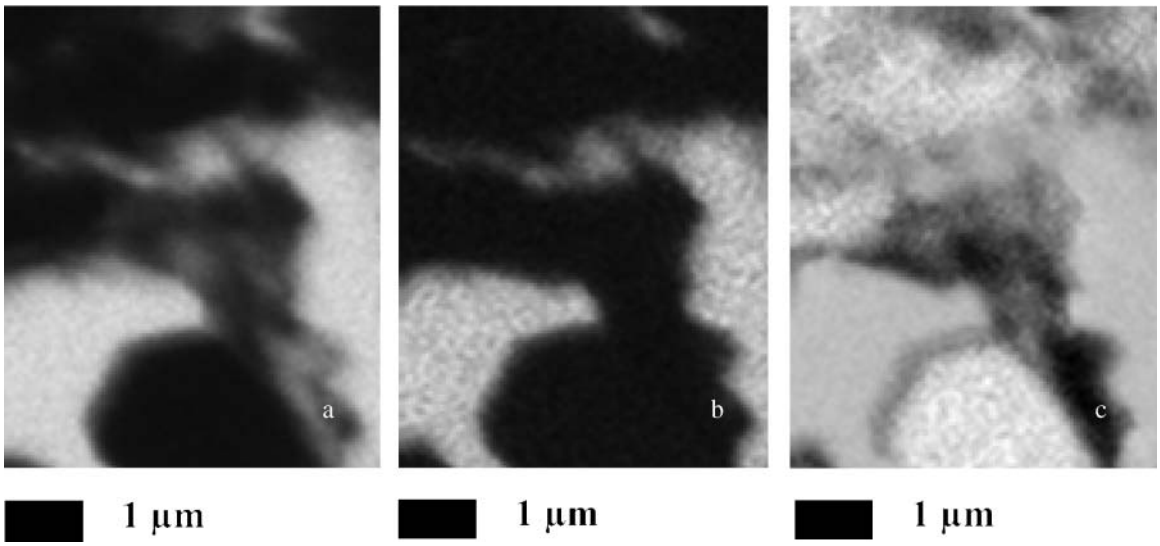

Fig. 2. STXM micrographs for an interior aggregate region taken (a) below 281 eV and (b) above 290 eV the carbon absorption edge. Contrast in the C and mineral density is shown in the ratio micrographs (c) calculated from–log [I/Io] where I = Σ (281 eV − 282 eV) and I*o* = Σ (290.6 eV − 291.5 eV).

Reproduced from Soil Science Society of America Journal. Published by Soil Science Society of America. All copyrights reserved.

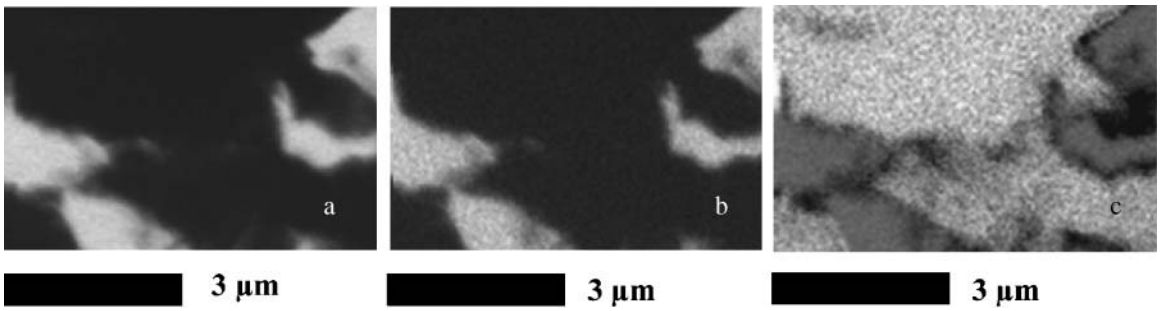

Fig. 3. STXM micrographs for an exterior aggregate region taken below (a) 281 eV and (b) above 290 eV the carbon absorption edge. Contrast in the C and mineral density is shown in the ratio micrographs (c) calculated from–log [I/Io] where I = Σ (281 eV − 282 eV) and I*o* = Σ (290.6 eV − 291.5 eV).

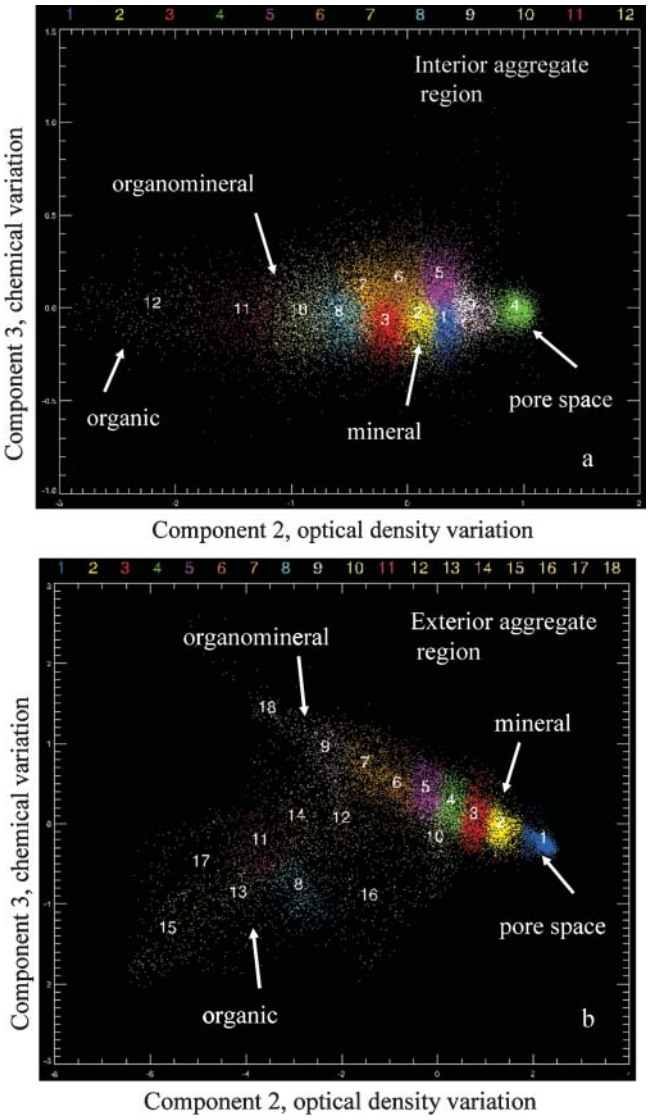

Fig. 4. Cluster pixel plots of components 2 and 3 show spectral characteristics of mineral and organic matter, color-coded for each cluster (color legend on top axis). Yellow color represents mineral cluster pixels separated from cluster pixels of organic and organomineral complexes by the blue (a) and green (b) clusters of pore space pixels. Pixel separation with an optical density gradient (axis component 2), distinguishes C chemical species in the organic or organomineral matter, and is noticeable only in (a) but not (b) on the axis component 3.

from the spectra search space. Although the OD values are now reported on a negative Y-axis scale, we interpret OD related to minerals as less negative (~0) and OD related to pore space as more negative (~−2.5). Following this revised procedure, we repeated cluster analyses on the significant components (s = 2, 3) to test for thematic contrast of the results. Pixels in the resulting plot of components were anchored near a mineral cluster center with clear expression of the contrast between organic matter,

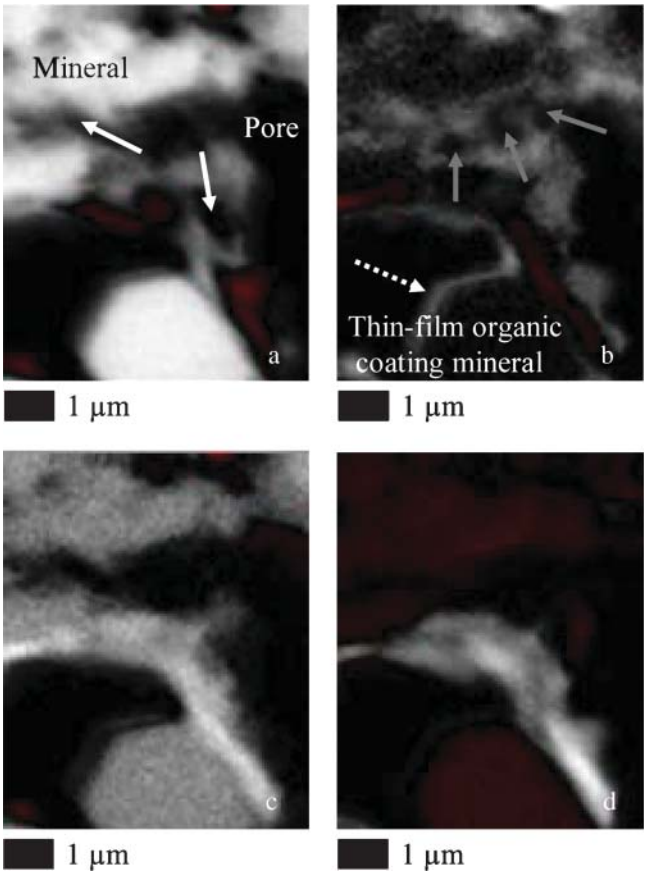

Fig. 5. Composition thickness maps of the main thematic regions in the interior of a micro-aggregate. Composition maps show (a) bright white regions of minerals, (b)organomineral complexes of carboxylic-C forms, (c) organomineral coatings of aromatic, (d) aliphatic-C forms, and particulate forms of aromatic-aliphatic-C. White arrows show small nanometer pores in mineral matrix. Grayscale arrows point at small nanometer pores in organomineral complex.

Reproduced from Soil Science Society of America Journal. Published by Soil Science Society of America. All copyrights reserved.

organomineral, and pore structures using both the 18 (Fig. 4a-interior) and 12 (Fig. 4b-exterior) classified regions.

Cluster Composition Thickness Maps

In the interior region of the microaggregate we completed an extensive evaluation of the cluster indices map (not shown), spectral pixel plots (Fig. 4a), and composition thickness maps (Fig. 5) to establish spatial interrelationships in the structural biogeocomplexity of the mineral-pore assemblage. Using NEXAFS, this mapping approach has been shown to reveal protein composition of sperm cells (Zhang et al., 1996) and spatial variations of BC oxidation (Lehmann et al., 2005). Compositional thickness maps displayed bright white regions that were associated with distinct and significant fitted spectra. In Fig. 5a, we observe variable nanoscale pore constrictions (>500 nm) and 2- to 5-μm large pore voids in dense mineral assemblage, stabilized by patchy occurrences of particulate or mineral-bound organic matter in both open and closed orifices. The exterior region of the microaggregate was explored across a much wider area (96 μm^2), providing a contiguous surface in the spatial connectivity of the aggregate from the outside pore region to the interior. The visible structures in the mineral-pore network and the location of mineral and organic matter are already revealed from 12 clusters (Fig. 4b) and these appear similar in their overall geometry to the interior regions of the microaggregate.

Spatial Distribution of Carbon Forms Inferred from Cluster Pixel Classification

C 1s-NEXAFS spectroscopy identified nano variability in mineral and C chemical composition of the mineral-pore assemblage. Gradations of the spectra in the C absorption region were captured by components $s = 2, 3$ after excluding $s = 1$ representing only average sample spectral characteristics and rejecting $s = 4$, when pixel to pixel signals were uncorrelated. From the cluster spectra we were able to distinguish organic matter bound to minerals along cavities, precipitating stable C assemblages which form mineral complexes that are separated by pore connectivity. The STXM images of the C density maps consistently revealed that the brightest image regions, which corresponded to the strongest C absorption signal (Lawrence et al., 2003), occurred within or along pore cavities but not between mineral layers such as may occur in marine environments (Ransom et al., 1997; Mayer et al., 2004). Four dominant thematic features in the microaggregate section were expressed as: (i) minerals, (ii) organomineral assemblages of predominantly oxidized C forms, (iii) particulate organic matter of aromatic, amide, aliphatic, carboxyl and carbonyl type C, and (iv) complex surface and internal pore networks (Fig. 5 and 6).

Organic Matter and Mineral Assemblage

Structurally, microaggregates were dominated by mineral matter. The mineral domain was displayed as a compact matrix consisting of sections that vary in optical density, whose spectral signal in the energy absorbance was ~2.5 (Fig. 5a and 6a). We observed mineral flakes that were loosely attached on the broken edges of more compact mineral matter. These assemblages of minerals appeared to bind to the organic matter that covered the compact mineral matter (Fig. 5c) providing early evidence for microaggregate formation in nanostructures. Such nano-aggregates may evolve into large agglomerates, forming the primary constituents that confer aggregation to highly weathered soils. According to Denef and Six (2005), this process leads to abiotic aggregate formation and reformation. Because the section of soil material is from an Oxisol, we further hypothesize that such nano-aggregation is likely initially mediated by abiotic-cationic mineral bonding (Kaiser et al., 2002). Evolving aggregates are then stabilized through geochemical controls such as wetting and drying cycles (Park and Smucker, 2005), salt mobility (Sollins et al., 1996), and pH charge dependence (Bronick and Lal, 2005), or geological time exposure (Trumbore, 1993).

Amelung et al. (2002) have examined a 50-nm depth region on soil surface particles using XPS and found organic matter to be concentrated at the particle surface. At the 50-nm depth, these authors possibly only measured organic matter bound on the surface as microfilms, excluding organic matter that is sequestered in surface breaking pores or localized by clogging internal connecting pores. Mikutta et al. (2004) reported a "pore-clogging" effect of AlOOH by dissolved organic C and Zimmerman et al. (2004) found large protein macromolecules to be excluded from the mineral surfaces through a "pore-filling" mechanism in marine sediments. Our findings

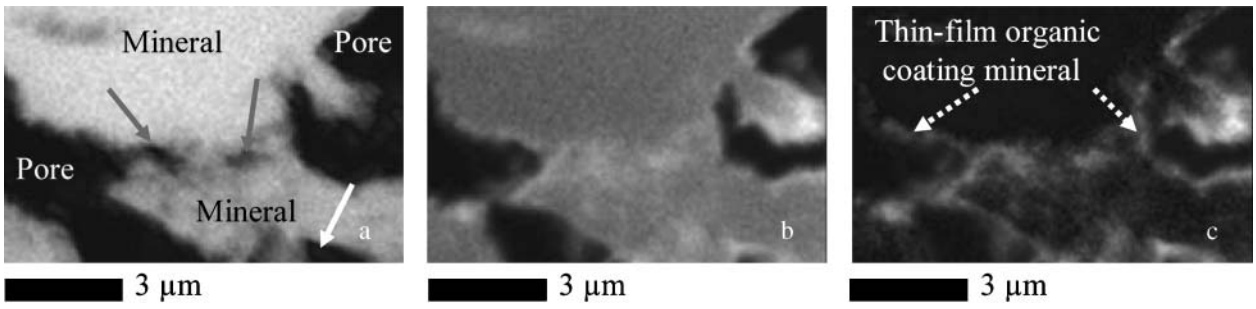

Fig. 6. Composition thickness maps of the main thematic regions at the exterior of a micro-aggregate. Composition maps show (a) bright white regions of minerals, (b) organomineral complexes of carboxylic-C forms, and (c) organomineral coatings of aromatic, carboxylic-C forms. Black arrows show small nanometer pores in mineral matrix. Black arrows point at small nanometer pores in organomineral complex.

Reproduced from Soil Science Society of America Journal. Published by Soil Science Society of America. All copyrights reserved.

support observations of organic matter stabilization on surface microfilms and in pore structures of the organo-mineral assemblage (Fig. 5b, 5c, 5d, 6b, and 6c).

Carbon Chemical Forms in Microaggregates

C 1s-NEXAFS spectra exhibited multiple peaks in the fine structure of the K-edge absorption region indicating the presence of multiple organic C functional moieties in the mineral-pore structures. Dominant C chemical forms visible in these nanostructures showed absorbance near 285.0, 286.0, 286.6, 287.3, 288.6, and 289.5eV energy regions. Their peak positions are designated 2, 3, 4, 5, 6, and 7, following spectra assignments published by past NEXAFS studies on known biomaterials (Table 2). Two peaks that appeared to be significant shifts in the absorbance energy attributed to aromatic-C and carbonyl-C, occurred near 286.0 and 289.7 eV. No transitions were recorded in the 284.3 eV region of low energy absorbance from saturated quinone type C. Organic matter in the interior region is most complex and required a large cluster search (18) to effectively classify C chemical composition regions (Fig. 4a). In contrast, no C chemical difference in the functional form was observed across spatial regions in the exterior region (Fig. 4b). The main C functional forms resolved in both sections can be summarized as:

1. Aromatic-C: protonated, alkylated, hydroxylated and amide substituted aromatic C (284.0 eV–287.1 eV): According to Table 2, the resonance at energy level 2, near 285.0 eV represents 1s→π* C = C of aromatic C (Boyce et al., 2002; Schäfer et al., 2003, Lehmann et al., 2005). Organic matter in pores inside the aggregate had a strong absorbance due to presence of phenyl rings and may indicate the existence of aromatic protein macromolecules (Brandes et al., 2004; Hitchcock et al., 2005). The peak intensity of aromatic-C declined significantly when organic matter was bound to minerals suggesting a transformation that oxidized C=C to COOH forms. Organic matter in exterior regions of the aggregate showed a weak 1s→π* C=C and no 1s→π* C–H indicating depleted aromatic-C and nearly no aliphatic-C forms. Carbon forms appearing at energy level 3 (Fig. 7f and 8f) suggest excitations due to 1s→π* C=N from N substitution in the phenyl ring (Ade and Urquhart, 2002; Brandes et al., 2004; Hitchcock et al., 2005). This functional form undergoes hydrolysis-reduction reactions to precipitate acidic COOH and basic NH_2 groups. In a study of 20 amino acids commonly occurring in soil biological material, Kaznacheyev et al. (2002) show that C=N bond structures are only found in histidine, (C=C) and arginine (no C=C). Although the C=N resonance occurs in the 286.0 to 286.5 eV energy region (Boese, 1996; Ade and Urquhart, 2002; Flynn et al., 2003), often overlapping with assignment to R-OH, work by Scheinost et al. (2001) suggests that the 1s→π* transition near 286.1 is not resonance from aromatic C bonded to OH. This resonance may instead originate from unsaturated aromatic-C (Lehmann et al., 2005) or C=O substituted aromatic-C (Cody et al., 1998). Flynn et al. (2003), who studied the C composition of interplanetary dust alluded to the ambiguity in this peak resonance arguing that both C=N and R–OH bonds are feasible assignments. We therefore recommend further experiments at the N 1s K-edge to fingerprint the C=N bond structures because organic matter in soil aggregates contains high N contents (9.8 g N kg^{-1} soil). Phenolic-C forms at energy level 4 were assigned 1s→π* C=C transitions of hydroxylated-C on the phenyl ring (Braun et al., 2005; Solomon et al., 2005). The absence of resonance due to phenols (286.6 eV-287.1 eV) and quinone type-C (284.0 eV) may point to evidence for lack of plant derived C from lignin degradation (Solomon et al., 2005).
2. Aliphatic-C (287.3 eV-287.6 eV) A pronounced resonance around 287.3 eV was assigned to 1s→π* transitions of C–H and appeared in the image of the interior regions of the aggregate (Fig. 7g and 7h). The presence of resonances in the aliphatic-C chain structure together with oxidized carboxyl and carbonyl-C suggested the occurrence of C forms in phospholipid fatty acids or chitin (Solomon et al., 2005) that may be residues from particulate C. The 1s→π* transition near 287.3 eV is also due to aliphatic-C of CH, CH_2, and CH_3 groups that may form non-polar termini that confer hydrophobic properties. Further experimentation is required to understand how nonpolarity establishes mineral coating of aromatic-aliphatic structures noticeable in Fig. 5c. Schreiber et al. (2000) attributed hydrophobicity in alkyl-thiol-based monolayers to the effect of phospholipid bilayers which in themselves

Table 2. Photon energy (eV) peak resonance assignment for organic C functional forms obtained from near edge absorption fine structure (NEXAFS) spectroscopy.

Peak regions	Photon energy	Carbon functional group forms†	References
1	284.3	Quinone-C, protonated aromatic-C	a, b, d, e i
2	284.9–285.5	Alkylated to carbonyl-substituted aromatic-C	a, b c, g, h
3	286.0–286.5	Unsaturated aromatic-C, C–N and C = N of N substitution in phenyl ring	a, d, e
4	286.5–287.1	Phenolic O–H, ketone O–C–O	c, d, e, f, h
5	287.3–287.6	Aliphatic C–H	a, b, i
6	287.7–288.8	Carboxyl-C, split features of C–C, C–H or COOH	a, c, e, g, i
7	289.3–289.8	Carbonyl-C, alcohol-C ether linkage R–O–R	d, e, f, i
8	289.8–290.0	Unassigned but probably organic C–O with traces of inorganic C–O	a

† Peak assignments for C 1s NEXAFS according to: a) Brandes et al. (2004); b) Braun et al. (2005); c) Cody et al. (1998); d) Hitchcock et al. (2005); e) Lehmann et al. (2005); f) Scheinost et al. (2001); g) Schäfer et al. (2003); h) Smith et al. (2001); and i) Solomon et al. (2005).

Reproduced from Soil Science Society of America Journal. Published by Soil Science Society of America. All copyrights reserved.

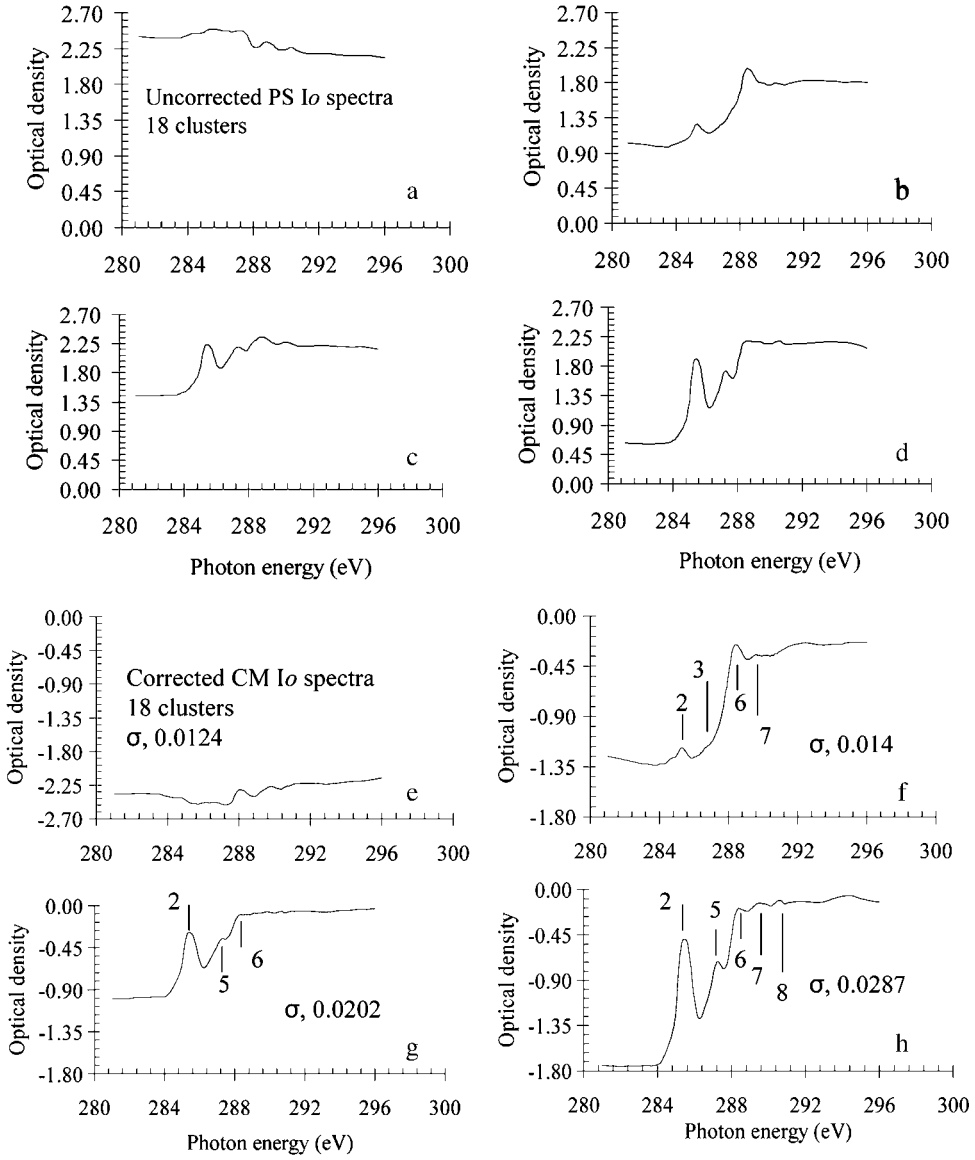

Fig. 7. Spectral signatures of the composition thickness maps of the interior area shown in Fig. 5, with both (a, b, c, and d) uncorrected PS-I*o* and (e, f, g, and h) CM-I*o* corrected spectra. Spectra (a) and (e) refer to mineral and pore space signatures, respectively. Spectra b and c show elevated optical density as a result of absorbance by mineral matter. Residual errors for the fitted spectra e, f, g, and h are shown with their root variance, σ.

are primary constituents of biological membranes (Benzerara et al., 2004). Therefore, we postulate particulate organic matter exhibiting 1s→π* C=C and 1s→π* C–H to in part, indicate structures and debris of re-synthesized C possibly of microbial membranes, tissue and residues.

3. Carboxyl-C (287.7 eV-288.8 eV): The strong absorption band near 288.6 eV was assigned to a 1s→π* COOH transition of carboxylic-C (Cody et al., 1998; Boyce et al., 2002; Schäfer et al., 2003; Lehmann et al., 2005). The characteristic carboxyl phenyl ring manifested a 0.3 eV energy shift on the C=O bond, down to 288.3 eV, which indicates the presence of carboxyamides (Lawrence et al., 2003; Benzerara et al., 2004; Brandes et al., 2004). Carbon chemical forms dominated by oxidized C are characterized by polar carboxyl-C absorption near 288.6 eV representing aliphatic rather than aromatic acids (Kaznacheyev et al., 2002). The peaks in both sections were broad signifying the presence of both amide and polysaccharide carboxyl-C (Benzerara et al., 2004). Oxidized organic matter interacted as a discontinuous thin film-type layer through binding in pore cavity regions on the mineral surface (Fig. 5b and 6c). Transmission electron microscopy has shown the existence of monolayers to explain the binding of natural organic matter to clay surfaces in marine sediments (Ransom et al., 1997) but further examination (Brandes et al., 2004; Mayer et al., 2004) now highlights a preferential and patchy location of organic matter in the mineral-pore complex. Our findings partly agree with Brandes et al. (2004) and Mayer et al. (2004), supporting observations for a patchy occurrence of organic matter on minerals. In addition to patchy location, we also observed a thin film of organic

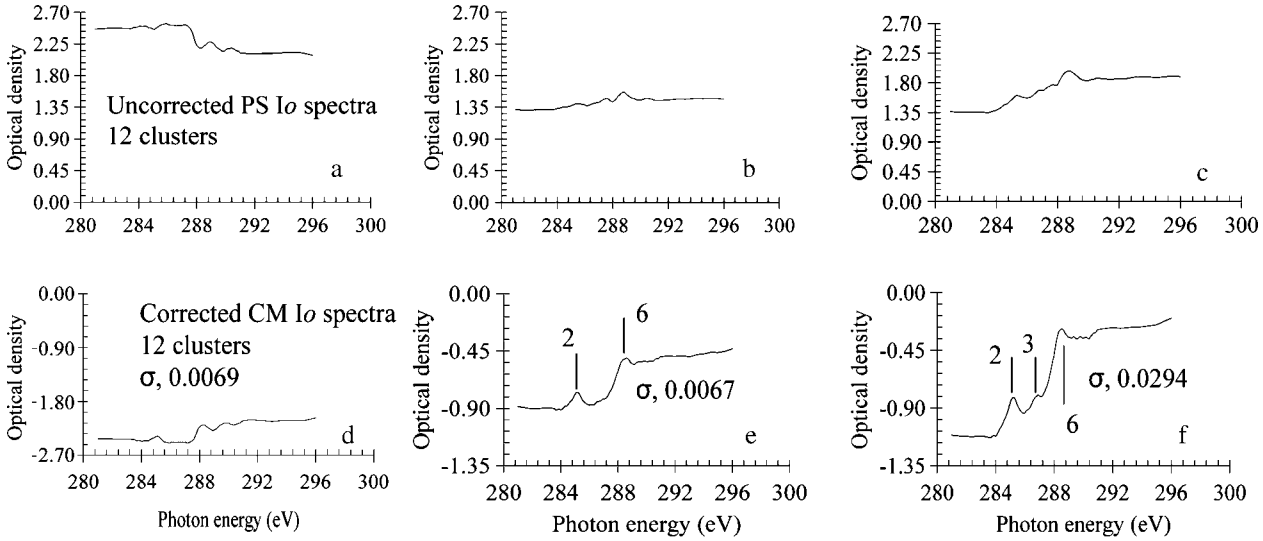

Fig. 8. Spectral signatures of the composition thickness maps of the exterior area shown in Fig. 6, with both (a, b and c) uncorrected PS-Io and (d, e and f) CM-I*o* corrected spectra. Spectra (a) and (d) refer to mineral and pore space signatures, respectively. Spectra (b), (c), (e), and (f) show elevated optical density as a result of absorbance by mineral matter. Residual errors for the fitted spectra (d), (e), and (f) are shown with their root variance, σ.

coating but not uniform monolayers, confirming that organic matter in soil microaggregates may be stabilized as patchy thin films on surfaces. The functional properties of protonated-deprotonated ($COOH/COO^-$) carboxyl termini visible in the spectrum of both regions (Fig. 7f, 8e, and 8f) indicates oxidative degradation under acidic conditions. Orientation in C binding, common to self-assembled layers, involving hydroxyl–OH and alkyl–CH groups may confer hydrophilic and hydrophobic termini (Schreiber et al., 2000), causing organic matter to either coat surfaces (Fig. 5c), or clog mineral pores (Fig. 6b).

4. Carbonyl-C (289.3 eV–289.6 eV): The sharp absorption band near 289.5 eV corresponds to the 1s→3p, σ* of C=O groups (Cody et al., 1998; Flynn et al., 2003) primarily representing polysaccharides, some aliphatic ethers and alcohol-C (Boyce et al., 2002; Scheinost et al., 2001). There was a visible shift to higher energy absorption resulting in 1s→σ* excitation of C=O (289.8 eV) specifically for organic matter clogging mineral pores or coating pore cavities. This peak shift maybe due to the inductive effect of 2 oxygen atoms adjacent to the carbonyl group (Boese et al., 1997; Smith et al., 2001), whose charge environment shows a band of O-substituted sp^3-hybridized C (Boyce et al., 2002) close to the ionization threshold (290 eV). The presence of the 1s→σ* C=O can be used to distinguish between protein-nucleic acid C=O and polysaccharide C–O in carboxylic groups of organic matter (Benzerara et al., 2004). We therefore find the occurrence of aromatic, aliphatic, and acidic carboxyl functional groups to provide evidence that microaggregates may be stabilized by protein (C=C, C=N, C=O), lipid (C–H, COOH), and polysaccharide (C–H, C–OH) organomineral complexes of organic matter in soil.

Implications for Modeling Soil Organic Matter Dynamics

Having examined the nanoscale spatial attributes of the C chemistry in microaggregates, we offer comments that may help to improve current models that describe interrelationships among the structural components in aggregate formation-deformation dynamics: i) there is merit to resolve preference for organic matter binding mainly to pore cavities where current models assume dominance of organic matter-mineral mixing in the organomineral complex; ii) we need to further investigate the relationship between clay contents and pore geometry with respect to C chemical adsorption and microbial access where models draw correlations between organic matter and soil texture as protective capacities; and iii) there is need to elucidate the affinity of polar hydrophilic COOH to complex with minerals while particulate non-polar aromatic and aliphatic-C structures are not complexed but rather coated by minerals, leading to geophysical occlusion of C.

CONCLUSIONS

Using STXM and C 1s-NEXAFS, we were able to visualize for the first time, an undisturbed intact microaggregate assembly and to resolve C functional forms at spatial resolutions that have not been feasible up to now with established methodological approaches. We have observed oxidized carboxyl-C to coat the mineral surface or clog pores. Hydrophobic aromatic and aliphatic-C was confined between mineral assemblages exhibiting encrustation or geophysical occlusion in 2- to 5-μm pore spaces. The chemical form of mineral-associated organic matter appeared to be significantly altered between exterior and interior regions. Organic matter in exterior regions was highly processed; containing more carboxyl-C relative to aromatic-C. Organic matter in interior regions was more complex and contained

Reproduced from Soil Science Society of America Journal. Published by Soil Science Society of America. All copyrights reserved.

Reproduced from Soil Science Society of America Journal. Published by Soil Science Society of America. All copyrights reserved.

significant amounts of aromatic and aliphatic-C. In this study, it is evident that the role of chemical adsorption for C stabilization in microaggregates of soils dominated by 1:1 clay minerals may be diminished due to organic matter retention in pores. Mineral surface flaking was noticeable in pore regions and the scale of primary particle intimacy for nano-aggregate formation-deformation is below the current scales of 20- to 250-μm postulated in many of the existing aggregation models. These findings provide only the first insights into C stabilization processes occurring in mineral-pore assemblages. Further STXM and NEXAFS studies incorporating N and O K-edge experiments are necessary to gain a complete understanding of the biogeocomplexity of soil microaggregates and their role in global C cycling.

ACKNOWLEDGMENTS

This study was funded by the Coupled Natural and Human Systems Program of the Biocomplexity Initiative of the NSF under grant BCS-0215890. The NEXAFS spectra were obtained from the National Synchrotron Light Source (NSLS), Brookhaven National Laboratory, at the Beamline X-1A1 developed by the research group of Janos Kirz and Chris Jacobsen at SUNY, Stony Brook, with support from the Office of Biological and Environmental Research, U.S. DoE under contract DE-FG02-89ER60858, and the NSF under grants DBI-9605045 and ECS-9510499. Many thanks to Joseph Njeri, Lawrence Lanogwa and Wilson Okila for help in soil sample procurement and to Yuanming Zhang at the Cornell Center for Materials Research for invaluable support during microtome cryo-sectioning.

REFERENCES

Ade, H., and S.G. Urquhart. 2002. NEXAFS spectroscopy and microscopy of natural and synthetic polymers. p. 285–355. *In* T.K. Sham (ed.) Chemical applications of synchrotron radiation. World Scientific Publishing, River Edge, NJ.

Ade, H., X. Zhang, S. Cameron, C. Costello, J. Kirz, and S. Williams. 1992. Chemical contrast in x-ray microscopy and spatially resolved XANES spectroscopy of organic specimens. Science 258:972–975.

Albee, P.B., G.C. Stockman, and A.J.M. Smucker. 2000. Extraction of pores from microtomographic reconstructions of intact soil aggregates. ANL/MCS-P791–0200. Mathematics and Computer Sci. Div. Argonne Natl. Lab., Argonne, IL.

Amelung, W., K. Kaiser, G. Kammerer, and G. Sauer. 2002. Organic carbon at soil particle surfaces-evidence from X-ray photoelectron spectroscopy and surface abrasion. Soil Sci. Soc. Am. J. 66: 1526–1530.

Beauchemin, S., D. Hesterberg, and M. Beauchemin. 2002. Principal component analysis approach for modeling sulfur K-XANES spectra of humic acids. Soil Sci. Soc. Am. J. 66:83–91.

Benzerara, K., T.H. Yoon, T. Tyliszczak, B. Constantz, A.M. Spormann, and G. Brown. 2004. Scanning transmission X-ray microscopy study of microbial calcification. Geobiology 2:249–259.

Blanco-Canqui, H., and R. Lal. 2004. Mechanisms of carbon sequestration in soil aggregates. Crit. Rev. Plant Sci. 23:481–504.

Boese, J.M. 1996. X-ray absorption near edge structure of amino acids and peptides. M. A. thesis. Department of Physics, State University of New York. Stony Brook NY.

Boese, J., A. Osanna, C. Jacobsen, and J. Kirz. 1997. Carbon edge XANES spectroscopy of amino acids and peptides. J. Electr. Spectr. Rel. Phen. 85:9–15.

Boyce, C., G. Cody, M. Feser, C. Jacobsen, A. Knoll, and S. Wirick. 2002. Organic chemical differentiation within fossil plant cell walls detected with x-ray spectromicroscopy. Geology 30:1039–1042.

Brandes, J.A., C. Lee, S. Wakeham, M. Peterson, C. Jacobsen, S. Wirick, and G.D. Cody. 2004. Examining marine particulate organic matter at sub-micron scales using scanning transmission X-ray microscopy and carbon X-ray absorption near edge structure spectroscopy. Mar. Chem. 92:107–121.

Braun, A., F.E. Huggins, N. Shah, Y. Chen, S. Wirick, S.B. Mun, C. Jacobsen, and G.P. Huffman. 2005. Advantages of soft X-ray absorption over TEM-EELS for solid carbon studies- a comparative study on diesel soot with EELS and NEXAFS. Carbon 43:117–124.

Bronick, C.J., and R. Lal. 2005. Soil structure and management: A review. Geoderma 124:3–22.

Cody, G.D., H. Ade, S. Wirick, G.D. Mitchell, and A. Davis. 1998. Determination of chemical-structural changes in vitrinite accompanying luminescence alteration using C-NEXAFS analysis. Org. Geochem. 28:441–455.

Denef, K., and J. Six. 2005. Clay mineralogy determines the importance of biological versus abiotic processes for macroaggregate formation and stabilization. Eur. J. Soil Sci. 56:469–479.

Elliott, E.T., K. Paustian, and S.D. Frey. 1996. Modeling the measurable and measuring the modelable: A hierarchical approach to isolating meaningful soil organic matter fractionations. p. 161–179. *In* D.S. Powlson et al. (ed.) Evaluation of soil organic matter models using existing long-term datasets. Springer-Verlag, Berlin. Germany.

Flynn, G.J., L.P. Keller, M. Feser, S. Wirick, and C. Jacobsen. 2003. The origin of organic matter in the solar system: Evidence from the interplanetary dust particles. Geochim. Cosmochim. Acta 67: 4791–4806.

Guggenberger, G., B.T. Christensen, and W. Zech. 1994. Land use effects on the composition of organic matter in particle-size separates of soil I. Lignin and carbohydrate signature. Eur. J. Soil Sci. 45:449–458.

Hitchcock, A.P., C. Morin, Y.M. Heng, R.M. Cornelius, and J.L. Brash. 2002. Towards soft X-ray spectromicroscopy of biomaterials. J. Biomat. Sci. Polymer Ed. 13:919–938.

Hitchcock, A.P., H.D. Stöver, L.M. Croll, and R.F. Childs. 2005. Chemical mapping of polymer microstructure using soft X-ray spectromicroscopy. Austr. J. Chem. 58:423–432.

Jacobsen, C., S. Wirick, G. Flynn, and C. Zimba. 2000. Soft X-ray spectroscopy from image sequences with sub-100 nm spatial resolution. J. Microsc. 197:173–184.

Kaiser, K., K. Eusterhues, C. Rumpel, G. Guggenberger, and I. Kögel-Knabner. 2002. Stabilization of organic matter by soil minerals-investigations of density and particle-size fractions of two acid forest soils. J. Plant Nutr. Soil Sci. 165:451–459.

Kaznacheyev, K., A. Osanna, C. Jacobsen, O. Plashkevych, O. Vahtras, H. Ågren, V. Carravetta, and A.P. Hitchcock. 2002. Inner-shell absorption spectroscopy of amino acids. J. Chem. Phys. 106:3153–3168.

Koprinarov, I.N., A.P. Hitchcock, C. McCrory, and R.F. Childs. 2002. Quantitative mapping of structured polymeric systems using singular value decomposition analysis of soft X-ray images. J. Phys. Chem. B 106:5358–5364.

Krull, E.S., E.A. Bestland, and W.P. Gates. 2002 Soil organic matter decomposition and turnover in a tropical Ultisol: Evidence from $\delta^{13}C$, $\delta^{15}N$ and geochemistry. Radiocarbon 44:93–112.

Lawrence, J.R., G.D.W. Swerhone, G.G. Leppard, T. Araki, X. Zhang, M.M. West, and A.P. Hitchcock. 2003 Scanning transmission x-ray, laser scanning and transmission electron microscopy mapping of the exopolymeric matrix of microbial biofilms. Appl. Environ. Microbiol. 69:5543–5554.

Lehmann, J., B. Liang, D. Solomon, M. Lerotic, F. Luizão, J. Kinyangi, T. Schäfer, S. Wirick, and C. Jacobsen. 2005. Near-edge X-ray absorption fine structure (NEXAFS) spectroscopy for mapping nano-scale distribution of organic carbon forms in soil: Application to black carbon particles. Global Biogeochem. Cycles 19:1013–1025.

Leifeld, J., and I. Kögel-Knabner. 2003. Microaggregates in agricultural soils and their size distribution determined by X-ray attenuation. Eur. J. Soil Sci. 54:167–174.

Lerotic, M., C. Jacobsen, T. Schäfer, and S. Vogt. 2004. Cluster analysis of soft x-ray spectromicroscopy data. Ultramicroscopy 100:35–57.

Mayer, L.M., L.L. Schick, K.R. Hardy, R. Wagai, and J.F. McCarthy. 2004. Organic matter content of small mesopores in sediments and soil. Geochim. Cosmochim. Acta 68:3863–3872.

Mikutta, C., F. Lang, and M. Kaupenjohann. 2004. Soil organic matter clogs mineral pores: Evidence from ^{1}H-NMR and N_2 adsorption. Soil Sci. Soc. Am. J. 68:1853–1862.

Oades, J.M., and A.G. Waters. 1991. Aggregate hierarchy in soils. Austr. J. Soil Res. 29:815–828.

Park, E.J., and A.J.M. Smucker. 2005. Erosive strengths of concentric regions within soil macroaggregates. Soil Sci. Soc. Am. J. 69: 1912–1921.

Ransom, B., R.J. Bennett, R. Baerwald, and K. Shea. 1997. TEM study of in situ organic matter on continental shelf margins: Occurrence and the "monolayer" hypothesis. Mar. Geol. 138:1–9.

Schäfer, T., N. Hertkorn, R. Artinger, F. Claret, and A. Bauer. 2003. Functional group analysis of natural organic colloids and clay association kinetics using C (1s) spectromicroscopy. J. Phys. IV France. 104:409–412.

Scheinost, A.C., R. Kretzschmar, I. Christ, and C. Jacobsen. 2001. Carbon group chemistry of humic and fulvic acid: A comparison of C-1s NEXAFS and ^{13}C-NMR spectroscopies. p. 39–47. *In* E.A. Ghabbour and G. Davies (ed.) Humic substances: Structures, models and functions. Royal Soc. Chem., Gateshead, UK.

Schmidt, C., J. Thieme, U. Neuhäusler, C. Jacobsen, B. Kaulich, M. Salomée, and J. Susini. 2003. Spectromicroscopy of soil colloids. J. Phys. IV France. 104:405–408.

Six, J., H. Bossuyt, S. De Gryze, and K. Denef. 2004. A history of research on the link between (micro) aggregates, soil biota, and soil organic matter dynamics. Soil Tillage Res. 79:7–31.

Smith, A.P., S.G. Urquhart, D.A. Winesett, G. Mithchell, and H. Ade. 2001. Use of near-edge X-ray absorption fine structure spectromicroscopy to characterize multicomponent polymeric systems. Appl. Spectr. 55:1676–1681.

Sohi, S.P., N. Mahieu, J.R.M. Arah, D.S. Powlson, B. Madari, and J.L. Gaunt. 2001. A procedure for isolating soil organic matter fractions suitable for modeling. Soil Sci. Soc. Am. J. 65:1121–1128.

Soil Survey Staff. 2003. Keys to soil taxonomy. 9th ed. USDA-Soil Conservation Service, Pocahontas Press, Blacksburg, VA.

Sollins, P., P. Homann, and B.A. Caldwell. 1996. Stabilization and destabilization of soil organic matter: Mechanisms and controls. Geoderma 74:65–105.

Solomon, D., J. Lehmann, J. Kinyangi, B. Liang, and T. Schäfer. 2005. Carbon K-edge NEXAFS and FTIR-ATR spectroscopic investigation of organic carbon speciation in soils. Soil Sci. Soc. Am. J. 69:107–119.

Stöhr, J. 1992. NEXAFS spectroscopy. Springer series in surface sciences 25. Springer, Berlin, Germany.

Tisdall, J.M. 1996. Formation of soil aggregates and accumulation of soil organic matter. p. 57–96. In M.R. Carter and B.A. Stewart (ed.) Structure and organic matter storage in agricultural soils. CRC Press, Inc., Boca Raton, FL.

Tisdall, J.M., and J.M. Oades. 1982. Organic matter and water-stable aggregates in soils. J. Soil Sci. 33:141–163.

Trumbore, S.E. 1993. Comparison of carbon dynamics in tropical and temperate soils using radiocarbon measurements. Global Biogeochem. Cycles 7:275–290.

Wander, M.M. 2004. Soil organic matter fractions and their relevance to soil function, p. 67–102. *In* F. Magdoff and R. Weil (ed.) Advances in agroecology. CRC Press, Boca Raton, FL.

Warwick, T., K. Franck, J.B. Kortright, G. Meigs, M. Moronne, S. Myneni, E. Rotenberg, S. Seal, W.F. Steele, H. Ade, A. Garcia, S. Cerasari, J. Denlinger, S. Hayakawa, A.P. Hitchcock, T. Tyliszczak, J. Kikuma, E.G. Rightor, H.J. Shin, and B.P. Tonner. 1998. A scanning transmission X-ray microscope for materials science spectromicroscopy at the Advanced Light Source. Rev. Sci. Instrum. 69:2964.

Zhang, X., R. Balhorn, J. Mazrimas, and J. Kirz. 1996. Mapping and measuring DNA to protein ratios in mammalian sperm head by XANES imaging. J. Struct. Biol. 116:335–344.

Zimmerman, A.R., K.W. Goyne, J. Chorover, S. Komarneni, and S.L. Brantley. 2004. Mineral mesopore effects on nitrogenous organic matter adsorption. Org. Geochem. 35:355–375.

Reproduced from Soil Science Society of America Journal. Published by Soil Science Society of America. All copyrights reserved.